**P2.9** INFRASONIC ATMOSPHERIC PROPAGATION STUDIES USING A 3-D RAY TRACE MODEL

R. Michael Jones*
*Cooperative Institute for Research in Environmental Sciences, University of Colorado, Boulder, Colorado*

Emily S. Gu
*Science and Technology Corporation, Boulder, Colorado*

A. J. Bedard, Jr.
*National Oceanic and Atmospheric Administration, Environmental Technology Laboratory, Boulder, Colorado*

## 1. INTRODUCTION

One component of our efforts to evaluate the capabilities of a demonstration infrasonic network (ISNet) for tornado detection is to understand the impact of complex propagation paths. Although atmospheric attenuation is not significant at infrasonic frequencies (e.g. $10^{-8}$ dB/km compared to 5 dB/km at 2 kHz), atmospheric wind and temperature gradients can have important effects upon detection ability. For example, since the early 1900s, unusual distributions of sound energy around explosions have been documented.

### 1.1 *A Historical Perspective*

An explosion at Oppau, Germany on September 21, 1921 illustrates the effects of upper atmospheric temperature and wind profiles on sound propagation. In this case, these characteristics cause alternating zones of silence and audibility. From the center of the explosion, sound was heard up to 100 km away, whereas between 100 and 200 km, a "zone of silence" existed where no sound was detected. Beyond 200 km, sound was audible by most observers to the east and south, as depicted in Fig. 1.

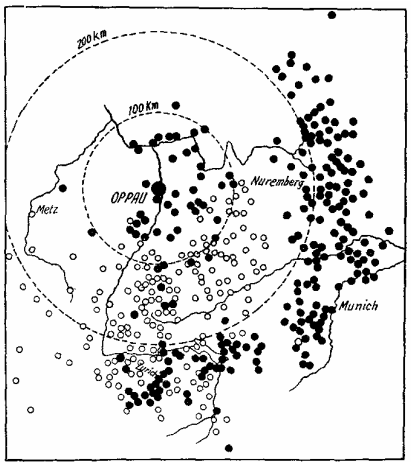


FIG. 1. Zones of audibility and silence for the explosion at Oppau, Germany. The black dots represent places where the sound was heard, and the white circles represent places where the explosion was not heard. (After Mitra, 1952)

* *Corresponding author address*: R. Michael Jones, University of Colorado, Cooperative Institute for Research in Environmental Sciences, Boulder, CO 80309-0216; e-mail: Michael.Jones@colorado.edu.

Thus, we ask the following questions:

- What factors affect long range infrasound propagation?
- What conditions constitute good and poor detectability at the earth's surface?
- What factors can produce bearing errors?
- How do these factors impact the design of infrasound networks?

### 1.2 *The Hamiltonian Ray-Tracing Program*

In an attempt to answer these questions, we applied a three-dimensional acoustic ray-tracing program (Jones, Riley, and Georges, 1986). The program had to be modified to run on more recent computers, and enhancements to initialize with arbitrary wind vectors and temperature profiles were added.

The ray-tracing program traces the three-dimensional paths of acoustic rays through model atmospheres by numerically integrating Hamilton's equations, which are a differential expression of Fermat's principle. Although Hamilton's equations are more familiar in mechanics, they can also be applied to wave propagation. In a high-frequency limit, waves behave like particles and travel along rays according to equations that exactly parallel those governing changes of position and momentum in mechanical systems.

Most past ray-trace simulations were performed on global scales of thousands of kilometers (e.g. studying sound propagation from nuclear explosions) or on "microscales" (e.g. addressing short-range problems involving noise pollution questions). The focus of this paper, however, is on ranges to 300 km, addressing intermediate-scale features of temperature and wind fields and their effects on the propagation of infrasound.

## 2. IDEAL PROPAGATION

Fig. 2 is an example of a visualization of ray paths for a sound source at an altitude of 13 km for a 1962 standard atmosphere with no wind (the "base case"). Note that there is a gap in rays striking the surface extending to 250 km. Also note the symmetry in the two directions for sound propagating outward from the source. If rays had been launched downward (at angles < 20°), there would have been an "audible" footprint extending outward to about 20 km from the source. However, winds and fine scale temperature structure can modify this picture significantly.

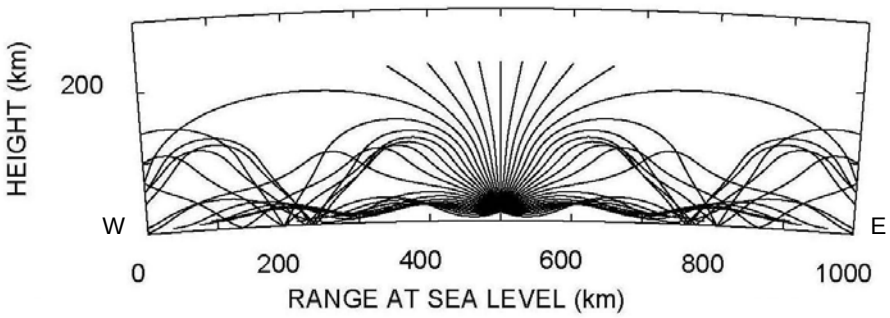


FIG. 2. Propagation with a standard temperature profile and no wind.

### 2.1 *Standard Temperature & 5 ms$^{-1}$ Wind*

Fig. 3 adds the effects of a climatological upper-level wind field. Note that the west to east wind fields create asymmetry in the picture with a zone of silence from 20 to 250 km to the west and from 20 to 200 km to the east. This figure explains some of the basic features of the zones of audibility and silence described in Fig. 1.

This case is similar to the base case, but now includes a background wind speed of 5 ms$^{-1}$ and a logarithmic wind profile of the atmospheric boundary layer neglecting Coriolis forces. The transmitter height and launch angles are identical to those in the base case, and rays are launched onto a flat terrain.

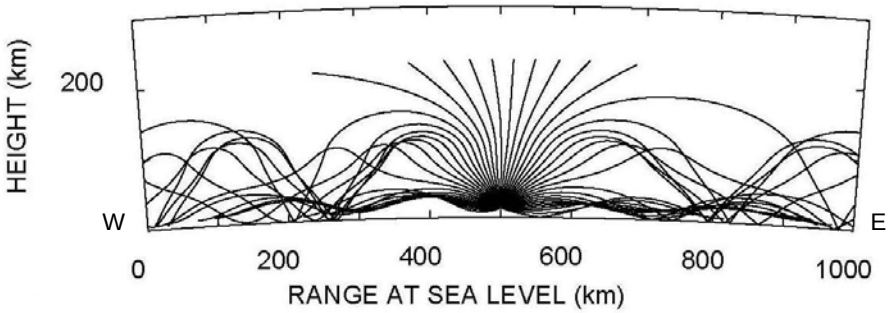


FIG. 3. Propagation with a standard temperature profile and 5 ms$^{-1}$ wind.

### 2.2 *Standard Temperature, No Wind, & A Fan Array*

Fig. 4 applies a distributed source model (fan array) instead of the point source model used in the base case simulations of figures 2 and 3. This source model assumes an isotropically radiating distributed source using discrete sources located from the surface to 2 km at 250 m intervals. The figure and ray trace visualization for a standard atmosphere with no wind shows robust propagation out to approximately 20 km.

This case has the standard temperature profile of the base case, along with no wind. Rays are launched from an azimuth angle of 90°, and the elevation angle varies from -8.5° to -12.5° and from 188.5° to 192.5° in 0.5° increments. Again, rays are launched onto a flat terrain.

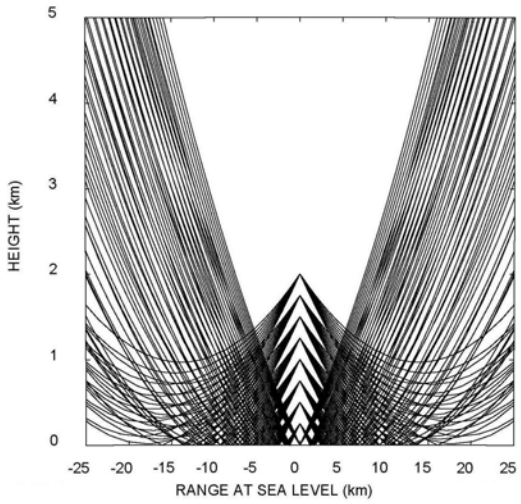


FIG. 4. Propagation with a standard temperature profile, no wind, and a transmitter fan array.

### 2.3 *Temperature Inversion, No Wind, & A Fan Array*

The significant features of this case are a low level thermal inversion at 2 km and an isothermal region below 2 km. There are multiple transmitters, equally spaced between 0 and 2 km at 250 m intervals. Rays are launched from an azimuth angle of 90° and from elevation angles ranging from -5° to 5° in 1° increments. The terrain is again flat.

From Fig. 5, it can be seen that the temperature inversion bends sound rays back towards the earth, allowing for detection virtually anywhere horizontally from the transmitter out to 200 km and beyond. The isothermal nature of this case allows for the rays to continue downward and reflect off the earth's surface. It is such fine-scale temperature or wind structure that creates variety in the ray paths of sound propagation.

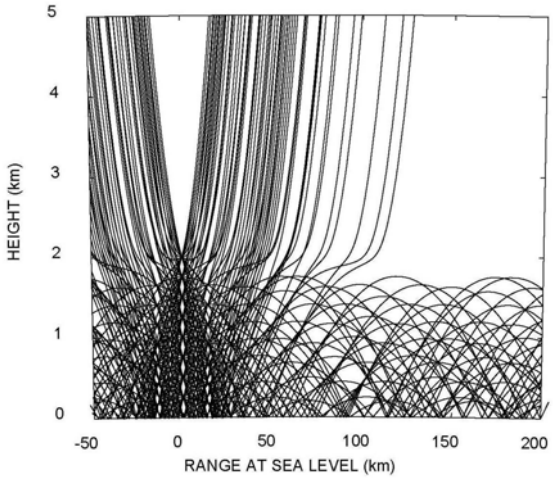


FIG. 5. Propagation with a thermal inversion at 2 km, isothermal below 2 km, no wind, and a transmitter fan array.

## 3. IDEAL VS. "REAL" PROPAGATION

### 3.1 *Gaussian Wind Jet*

Now we start to deal with more specific simulations. The first addresses the detection of infrasound by the Pueblo, CO ISNet system from a fire on July 19, 2003 at a range of 175 km, but no detection of infrasound at the Boulder Atmospheric Observatory (BAO) at a range of 30 km. A key factor in the atmospheric profile was the existence of north-to-south low-level flow, which we simulated as a Gaussian wind field of 10 $ms^{-1}$ centered at 3 km moving in the direction of Pueblo. The ray paths shown in Fig. 6 indicate that the lower level wind fields were critical to the detection at Pueblo and the lack of signal at Boulder even though the BAO is much closer than Pueblo. There was no significant inversion present for this case.

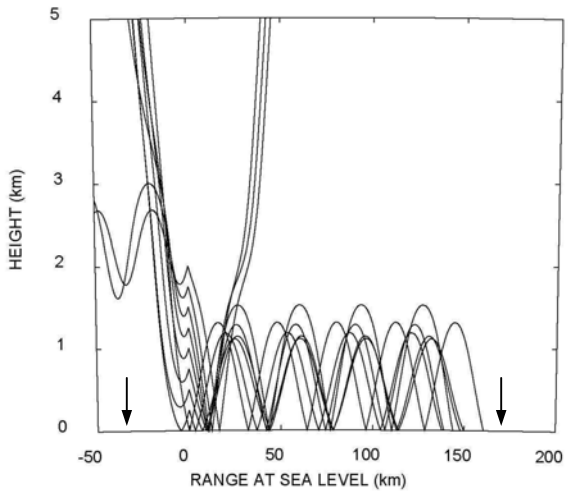


FIG. 6. Propagation with a Gaussian wind jet. The arrow at -30 km represents the location of the BAO, and the arrow at 175 km represents Pueblo.

### 3.2 *Sound Rays Passing Through a Mesocyclone*

Next, we examine the effect of a larger scale vortex on the propagation of sound from a tornado scale vortex. The mesocyclone is simulated by a counter-clockwise rotating Rankin-combined vortex with a maximum tangential wind speed of 20 $ms^{-1}$ at a radius of 5 km. In Fig. 7, the rays are presented in a horizontal plane with a tornadic sound source at the center of the mesocyclone. In this case, the ray paths are rotated, but no bearing errors would occur for stations receiving sound from the central source.

In Fig. 8, the tornadic source is located 20 km to the south of the mesocyclone. Only rays passing directly through the vortex are bent. Fig. 9 shows the rays passing through the mesocyclone in more detail.

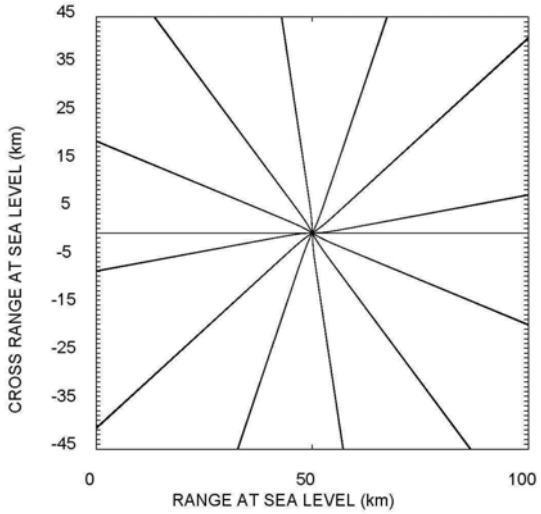


FIG. 7. Propagation through a mesocyclone. Ray paths are rotated, but no bearing errors occur.

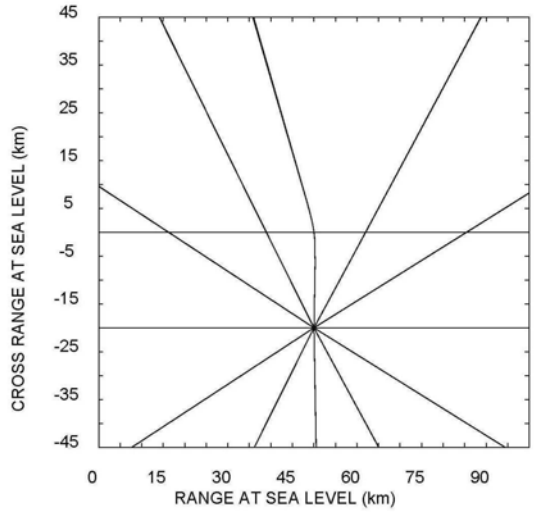


FIG. 8. Propagation through a mesocyclone. Only rays passing directly through the vortex are bent.

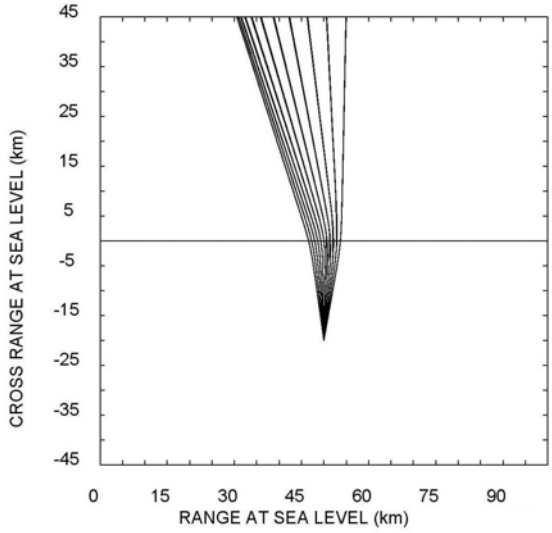


FIG. 9. Propagation through a mesocyclone. The azimuth angle varies from -5° to 5° in 1° increments.

## 4. TORNADIC CASE STUDIES

### 4.1 *Model for a Tornadic Sound Source*

In order to run the ray-tracing program to fit the temperature and wind profiles for individual cases, we first used a program to plot temperature, wind speed, and wind direction profiles that were obtained from radiosonde data archived by the Forecast Systems Laboratory (Fig. 10). Then, we made detailed analytical fits of the profile data in order to initialize the ray-trace runs (Figs. 11 & 12). In all these simulations, a tornadic sound source model was applied as described in section 2.2. A climatological wind profile was used to define the upper level temperature and winds (Georges & Beasley, 1976).

### 4.2 *May 11, 2004*

On May 11, 2004, there were seven reported tornadoes between 0004-0152 UTC in the counties of Weld (directly north of the BAO) and Elbert (northeast from Pueblo) in CO. The BAO detected signals from the direction of the Weld county tornado, and Pueblo detected sound from the direction of the tornadoes in Elbert county.

Note that the north-to-south propagating rays in Fig. 14 reach the surface to the south at about 100 km from the source, while the range is over 200 km for sound propagating to the north. The BAO was 53 km to the south of the tornado in Weld county and Pueblo was 119 km south of the tornadoes in Elbert county.

Beyond 20 km from the source, east-to-west propagating sound showed a zone of silence extending to over 200 km in both the east and west directions (Fig. 13).

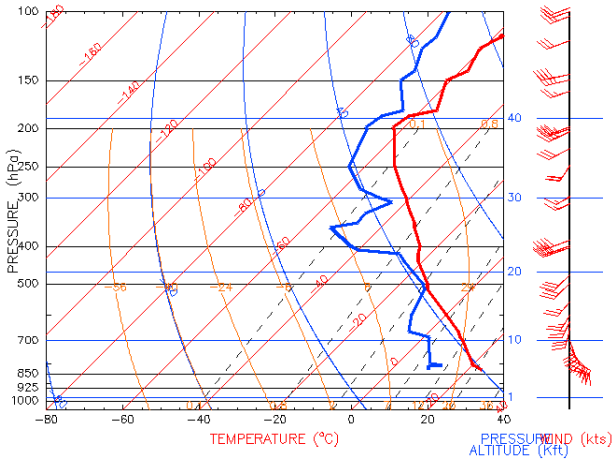


FIG. 10. May 11, 2004 (0000 UTC) temperature, wind speed, and wind direction profile.

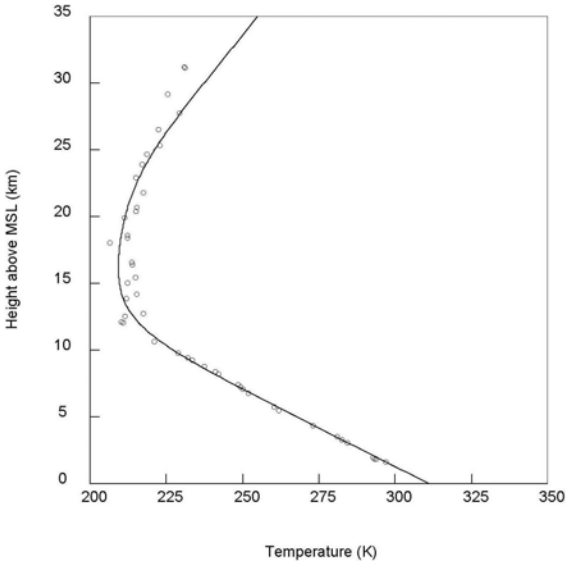


FIG. 11. May 11, 2004 (0000 UTC) temperature profile.

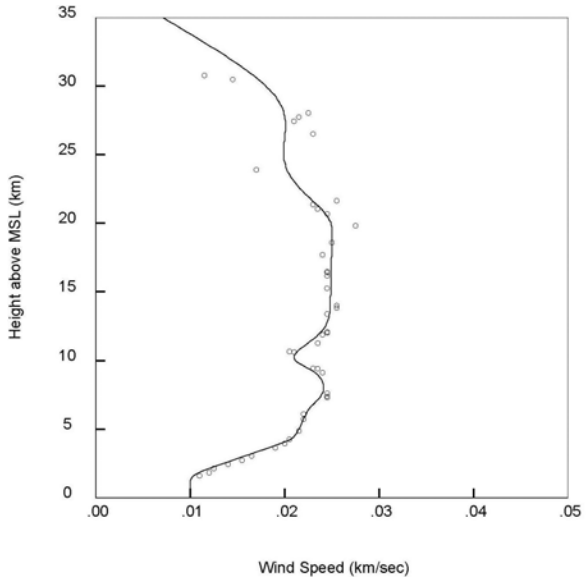


FIG. 12. May 11, 2004 (0000 UTC) wind speed profile.

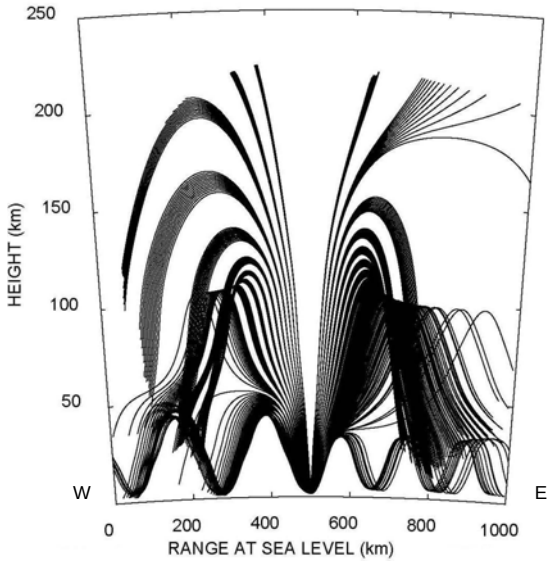


FIG. 13. East-to-west propagation with a May 11, 2004 profile.

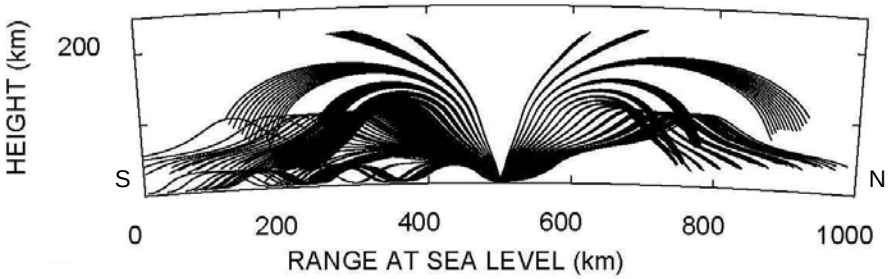


FIG. 14. North-to-south propagation with a May 11, 2004 profile. Rays are truncated due to limits of numerical processing.

### 4.3 *May 21, 2004*

The profile for May 21, 2004 showed stronger winds from the southwest above 500 mb (Fig. 15). This wind speed gradient and a weak inversion produced some trapping of rays at low levels for propagation towards the northeast (Fig. 16). Fig. 17 is an expanded view of the ray trace results, showing trapped rays between 2.5 and 5 km, which are predicted not to reach the surface. The three reported tornadoes were approximately 70 km to the east-northeast of the BAO. Weak signals were detected at the BAO during the period of the tornado reports. These signals appeared more clearly using a histogram-based detection algorithm, which is designed for identifying lower level, persistent signals.

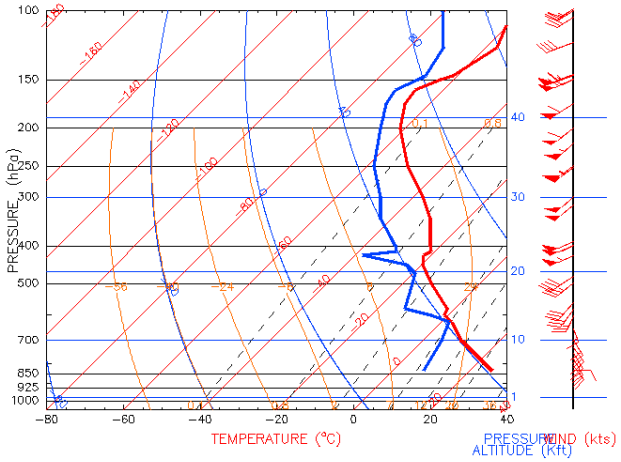


FIG. 15. May 21, 2004 (0000 UTC) temperature, wind speed, and wind direction profile.

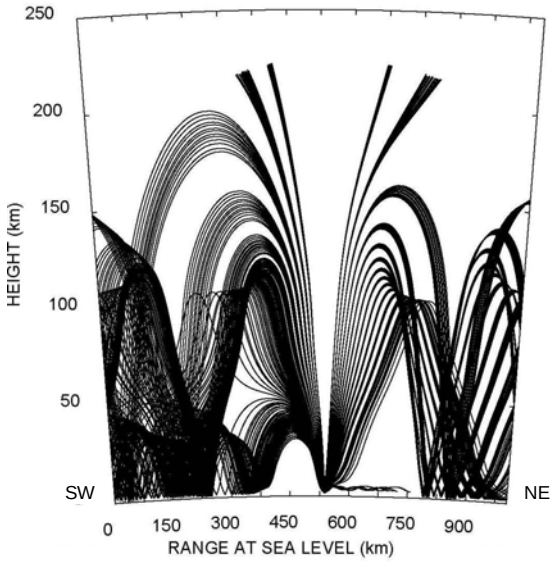


FIG. 16. Northeast-to-southwest propagation with a May 21, 2004 profile.

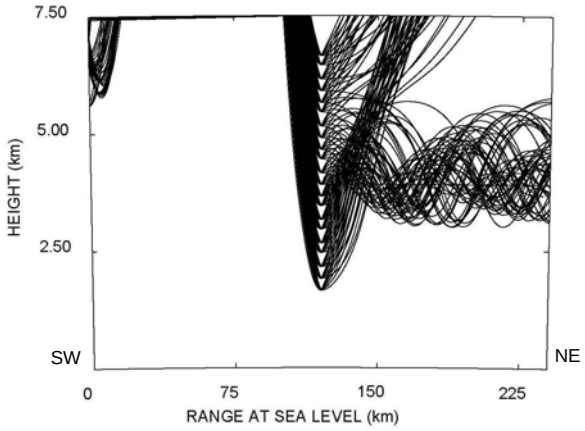


FIG. 17. A closer look at the northeast-to-southwest propagation with a May 21, 2004 profile. The ground is located 1.6 km (the elevation of the BAO in Colorado) above sea level.

### 4.4 *June 9-10, 2004*

For the ray-trace simulation on June 10, 2004 (Fig. 18), robust propagation conditions are predicted for both the east-to-west (Figs. 20 & 22) and north-to-south (Figs. 19 & 21) directions. These temperature and wind gradients combine to trap rays near the surface of the earth and prevent zones of silence. These conditions were favorable for the strong signal detections obtained at all three observatories. The BAO detected the movement of a cell to the east, while Goodland detected a cell to the northwest. Goodland detected signals from another system to the southeast moving northeast. All these systems involved tornado reports (BAO/Goodland) or showed evidence of rotation.

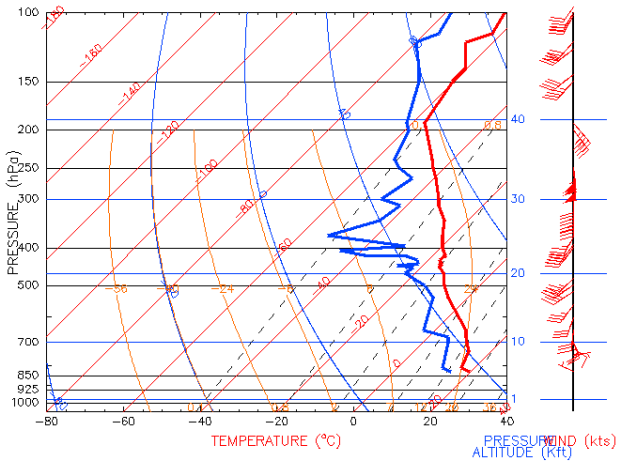


FIG. 18. June 10, 2004 (0000 UTC) temperature, wind speed, and wind direction profile.

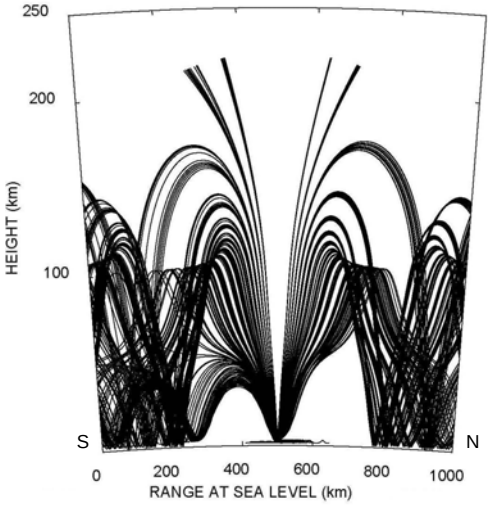


FIG. 19. North-to-south propagation with a June 10, 2004 profile.

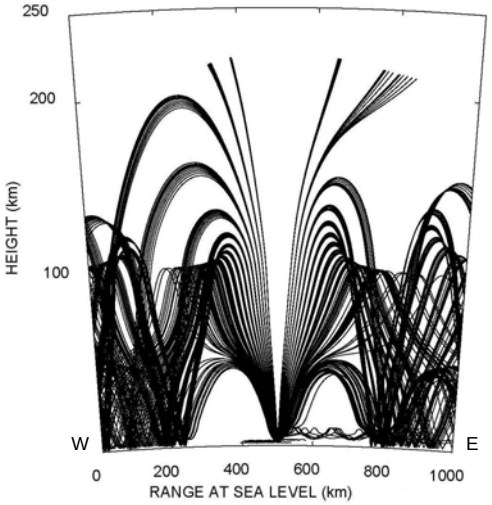


FIG. 20. East-to-west propagation with a June 10, 2004 profile.

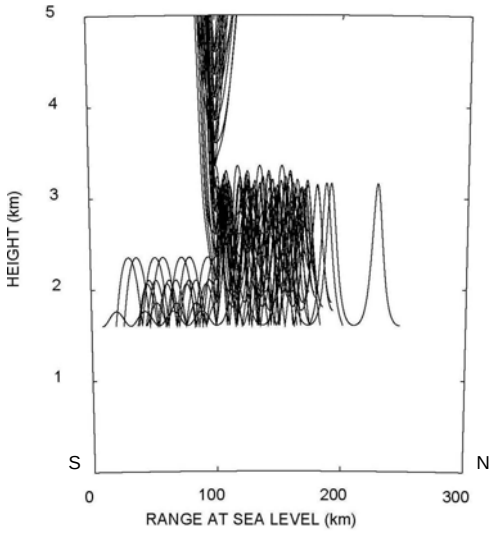


FIG. 21. A closer look at the north-to-south propagation with a June 10, 2004 profile. The ground is located 1.6 km (the elevation of the BAO in Colorado) above sea level.

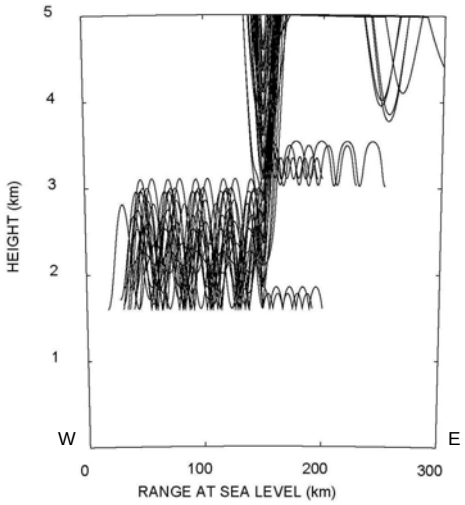


FIG. 22. A closer look at the east-to-west propagation with a June 10, 2004 profile. The ground is located 1.6 km (the elevation of the BAO in Colorado) above sea level.

### 4.5 *June 17, 2004*

The simulation of June 17, 2004 is another case indicating robust detection potential with no silent zone at the surface. There was an isothermal region near the surface and strong low-level directional wind shear (Fig. 23). Fig. 24 presents the east-to-west ray paths and Fig. 25 is on a finer scale. Fig. 25 shows the rays are trapped at the surface for both westward and eastward propagation. For this case, there was a tornado reported in far eastern Kansas. Signals were detected by the Goodland observing system.

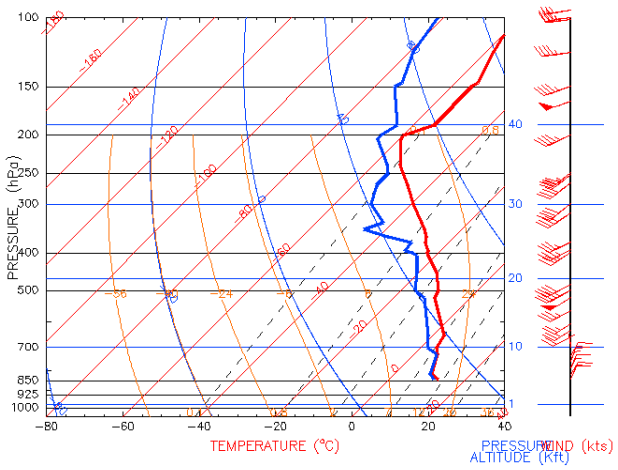


FIG. 23. June 18, 2004 (0000 UTC) temperature, wind speed, and wind direction profile.

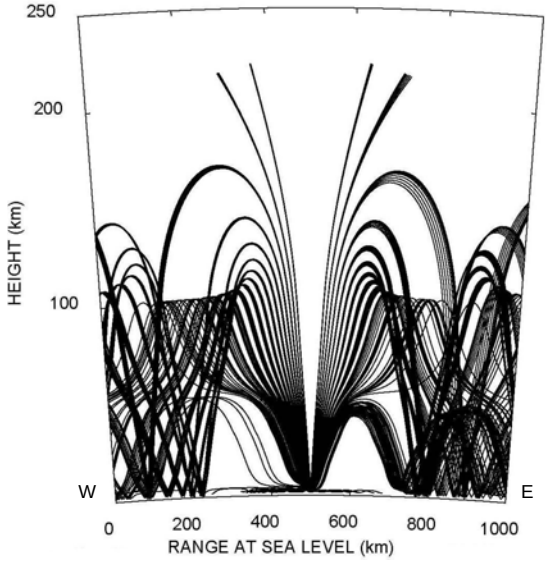


FIG. 24. East-to-west propagation with a May 21, 2004 profile.

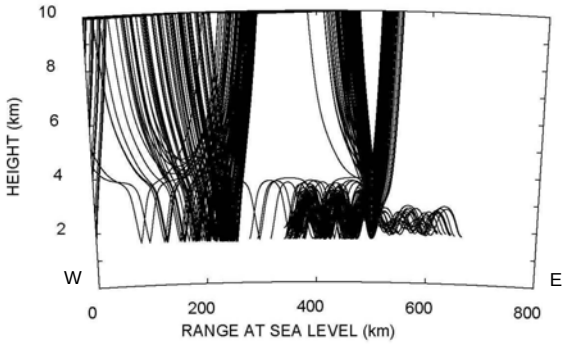


FIG. 25. A closer look at the east-to-west propagation with a May 21, 2004 profile. The ground is located 1.6 km (the elevation of the BAO in Colorado) above sea level.

## 5. SUMMARY & CONCLUDING REMARKS

Table 1 summarizes our key results from simulations preformed to date. A challenge remains to generalize these results for key situations. Our goals are to simulate infrasonic propagation around tornadic supercell and landspout environments. There is a need to define the zones of silence surrounding such situations to help evaluate detection potentials and guide network design.

Ray-trace simulations performed to date indicate the following:

- Robust propagation occurs under all conditions to 20 km from infrasonic sources.
- The upper level winds control the width of the silent region with the downwind distance extending to between 100 and 200 km. Distant propagation in the upwind direction is poor. Because the upper level winds are from east to west in the summer in the northern hemisphere, observatories to the west of tornadoes will be more effective at longer range detection.
- Lower-level wind gradients can trap rays, permitting sound to reach the surface for large regions in the downwind directions and causing zones of silence in the upwind directions.

Fig. 26 illustrates a concept for an infrasonic network design using simulation data appearing in the paper. Temperature inversions and near-surface isothermal layers permit good detectability in all directions for extended ranges.

| Situation | Region Near Source | Distant No Wind | Distant Upwind | Distant Downwind | Comments |
|---|---|---|---|---|---|
| Standard atmosphere & no wind | ± 20 km | 20 to 200 km symmetric zones of silence | | | |
| Standard atmosphere & upper level wind | ± 20 km | | 20 to 250 km zone of silence | 100 to 200 km zone of silence | Distant upwind propagation weak at long ranges |
| Inversion & Isothermal lower layer | No zone of silence | No zone of silence | No zone of silence | No zone of silence | |
| Source at center of mesocyclone | | | | | Ray rotation, but no bearing errors |
| Source 20 km south of mesocyclone | | | | | Bearing errors only for rays passing through mesocyclone core |
| Low-level Gaussian wind field of 10 $ms^{-1}$ | | | Upward refraction produces zones of silence | No zone of silence | |
| May 11, 2004 case study | ± 20 km | | 20 to 200 km zones of silence to both E and W | | 20 to 100 km to S, 20 to > 300 km to N zones of silence |
| May 21, 2004 case study | ± 20 km | | 20 to > 300 km zone of silence to the NE | 20 to 150 km zone of silence to the SW | Rays trapped at lower levels, but predicted not to reach the surface |
| June 9-10, 2004 case study | No zone of silence | | No zone of silence | No zone of silence | |
| June 17, 2004 case study | No zone of silence | | No zone of silence | No zone of silence | |

TABLE 1. Summary of key results of ray-trace simulations.

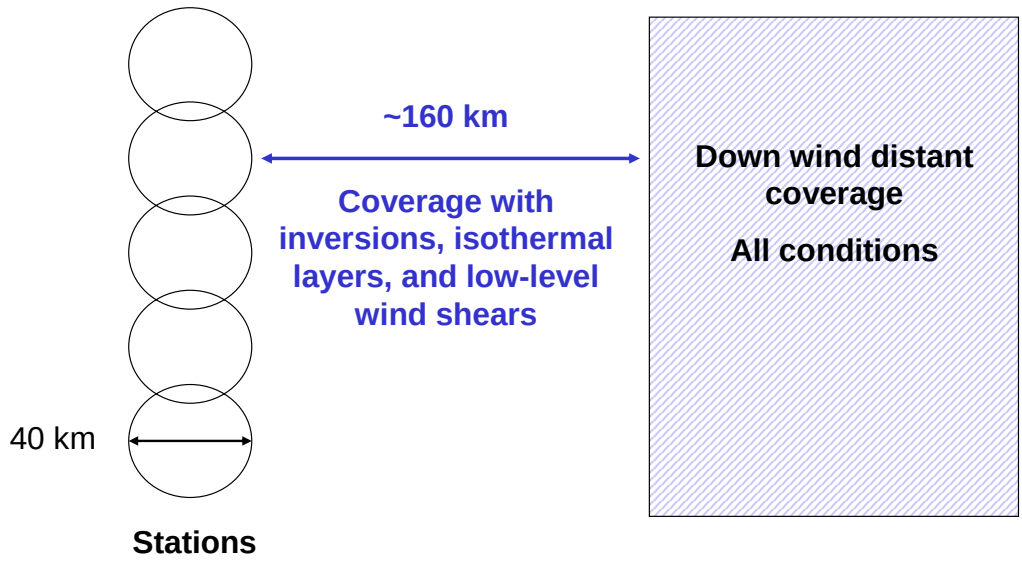


FIG. 26. A concept of the placement of infrasonic stations in an urban corridor based upon our numerical ray-trace simulations that would maximize detectability.

## 6. ACKNOWLEDGEMENTS

The authors would like to thank William Otto and Wendi Madsen for their assistance in upgrading the ray-trace program to be compatible with present-day compilers and loaders.

## 7. REFERENCES

Georges, T. M., and W. H. Beasley, 1976: Refraction of infrasound by upper-atmospheric winds. *J. Acoust. Soc. Am.*, **61**, 28-34.

Jones, R. M., J. P. Riley, and T. M. Georges, 1986: HARPA -- A versatile three-dimensional Hamiltonian ray-tracing program for acoustic waves in the atmosphere above irregular terrain. NOAA Special Report, 410 pp., GovDoc No. C55.602: H 18; GPO Item No. 207-C-1; PB87132031.

Mitra, S. K., 1952: *The Upper Atmosphere*. The Asiatic Society, 713 pp.